Universiteit Utrecht

Master Thesis

Phase Behavior Of Colloidal Elongated Dumbbells & Lollipops

January 31, 2017

Author:
A.L. Gabrielse
3279456

Supervisor:
Prof. Dr. Ir. M. Dijkstra

Daily supervisors:
Nikos Tasios
Simone Dussi

Acknowledgments

First and foremost, I have to thank my daily supervisors, Simone Dussi and Nick Tasios for their everyday assistance and dedicated involvement in the simulations, writing and presentation. I also would like to thank Marjolein Dijkstra for making this project possible and assisting me throughout this master thesis.

Abstract

We perform Monte Carlo simulations on hard elongated dumbbells and lollipops. The dumbbells are modeled as hard spherocylinders with a hard sphere attached at each end. For the lollipops one of these spheres is removed. Like in a system of hard spherocylinders we find that both shapes self-assemble into nematic and smectic liquid crystal phases. Our results show that the hard spheres destabilize the nematic phase with respect to the isotropic phase, whereas an increase in length of the particles increases the stability. Moreover, the spheres destabilize the smectic, AAA- and ABC-crystal ordering but give rise to the formation of a columnar phase. The existence of a cholesteric phase is studied by forcing the system in a cholesteric phase via a chiral potential. Simulation results are inconclusive, longer simulations are needed to equilibrate the systems further. A possible smectic-c phase is observed for the hard lollipops.

Contents

1 Introduction

1.1 Liquid Crystals

Substances can generally be found in three different phases of matter: Solids, liquids and gases. For certain materials there is a range between the crystal (solid) and liquid phase in which liquid crystal phases occur. These liquid crystalline materials tend to flow like a liquid but due to partial ordering of the particles also show some of the optical properties of a solid. The different phases of matter can be distinguished in terms of the different microscopic arrangement of their components. In a crystal the components are ordered on a three dimensional periodic lattice whereas isotropic liquids have no such order and can therefore flow freely. Liquid crystal phases consist of (anisotropic) particles that are orientationally ordered. However, the particle positions are not, or only partially, ordered. Liquid crystals can be found in nature [1] and in technological applications [2]. The three most common phases are the Nematic, Cholesteric and the Smectic phase. In the nematic phase the long axes of the particles are on average, aligned along a common direction and there is no positional order. Nematic liquid crystals can be aligned along an electric field which makes them very useful for liquid crystal displays (LCD's) [3]. Like the nematic phase, the cholesteric phase features no positional order and the particles are aligned along a common direction that twists in space in a helical manner. Cholesteric liquid crystals reflect different wavelengths of light depending on their pitch and can thus be used in thermometers [4]. In the smectic phase an additional positional ordering of the particles occurs in one dimension, i.e., the aligned particles form layers. This layered structure can form membranes that are similar to soap bubbles [5]. In this thesis we will also discuss the columnar phase. As the name suggests, in this phase particles form columns on a two dimensional crystal lattice.

1.2 Self-assembly

To understand how the liquid crystal phases are formed we first need to discuss its building blocks and mechanics. In this thesis we study the self-assembly of colloidal suspensions. Colloids can be defined as large insoluble particles in the size range between 1 nm and 1 μm. When dispersed in a solvent, the colloids constantly collide with the smaller particles of the solvent. Due to the thermal agitation of the solvent the colloids exhibit random trajectories also known as Brownian motion. Robert Brown observed this random motion in 1827 under a microscope studying pollen grains suspended in water [6]. Although any object will perform Brownian motion when suspended in a gas or liquid, particles larger then a few micrometer will not significantly be affected by these weak forces. Particles in the colloidal regime, unlike larger particles, are therefore continually in motion. Given sufficient equilibration time, this constant motion of colloidal particles allows them to self-assemble into a variety of phases [7].

A lot of research on the self-assembly of colloids has been performed. Theoretical predictions can be tested with computer simulations and eventually experimentally verified in the laboratory. For this thesis we will use computer simulations to mimic the phase behavior of radially symmetric elongated colloidal particles forming liquid crystals. One of the first studies using computer simulations was done in 1953 simulating hard spheres [8]. Hard spheres, driven by Brownian motion, are not allowed to overlap with each other but have no further interaction. Compressing the system from a low density leads to a transition from a fluid to a crystal phase. This spontaneous ordering can be explained by the minimization of the free energy

$$F = U - TS, \tag{1.1}$$

with internal energy U, temperature T and the entropy of the system S. In the case of hard particles the internal energy only depends on the temperature [9]. At a fixed temperature and density an increase in order can therefore only occur with an increase in entropy. Boltzmann's microscopic expression of entropy

$$S = k_b \ln \Omega, \tag{1.2}$$

says that the entropy is proportional to the logarithm of the number of states Ω of the system times the Boltzmann constant k_b. In the case of a crystal of hard spheres, for example, the number of microscopic

states is determined by the free volume available to the particles. By spontaneously ordering into a crystal the particles increase the free volume and entropy, thus minimizing the free energy of the system. Simulations of hard spherocylinders [10], cylinders with two spherical caps, shows nematic and smectic phases.

1.3 Dumbbells and lollipops

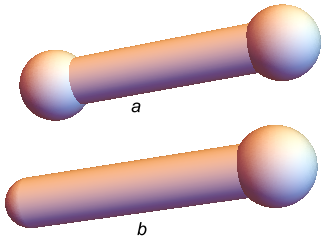

Figure 1.1: Graphical depiction of a Dumbbell (a) and a Lollipop (b) particle.

New experimental techniques provide possibilities for synthesizing colloidal particles in a diversity of shapes. Gold nanoparticles can be fabricated into dumbbell-like structures [11]. Polymer growth on silica rods can produce lollipop-like structures [12]. Results of these experiments are shown in Fig. 1.2. Experimentalists, or colloid scientists, can make real systems from these colloidal particles, that behave like hard particles used in simulations. Simulations can therefore provide an important insight into the phase behavior of these colloidal systems. Here we report simulations on the phase behavior of elongated hard dumbbells and lollipops. Elongated dumbbells consist of a cylinder with two identical spheres on its two ends. For the lollipops, one of the spheres has the same diameter as the cylinder. A graphical representation of these particles is shown in Fig. 1.1. In a study from 2011 by de las Heras et al. [13], hard top-shaped particles were studied. These top-shaped particles, like the dumbbells and lollipops consist of a spherocylinder but with a sphere at its center. De las Heras et al. report the role of the sphere on the stability of the columnar phase. For this thesis we will study the columnar phase for a system of hard dumbbells and lollipops. In his book on liquid crystals, de Gennes [14] suggests the possibility of a cholesteric nematic phase for dumbbell-like particles. Motivated by this, we will test the stability of this cholesteric ordering for the elongated hard dumbbells.

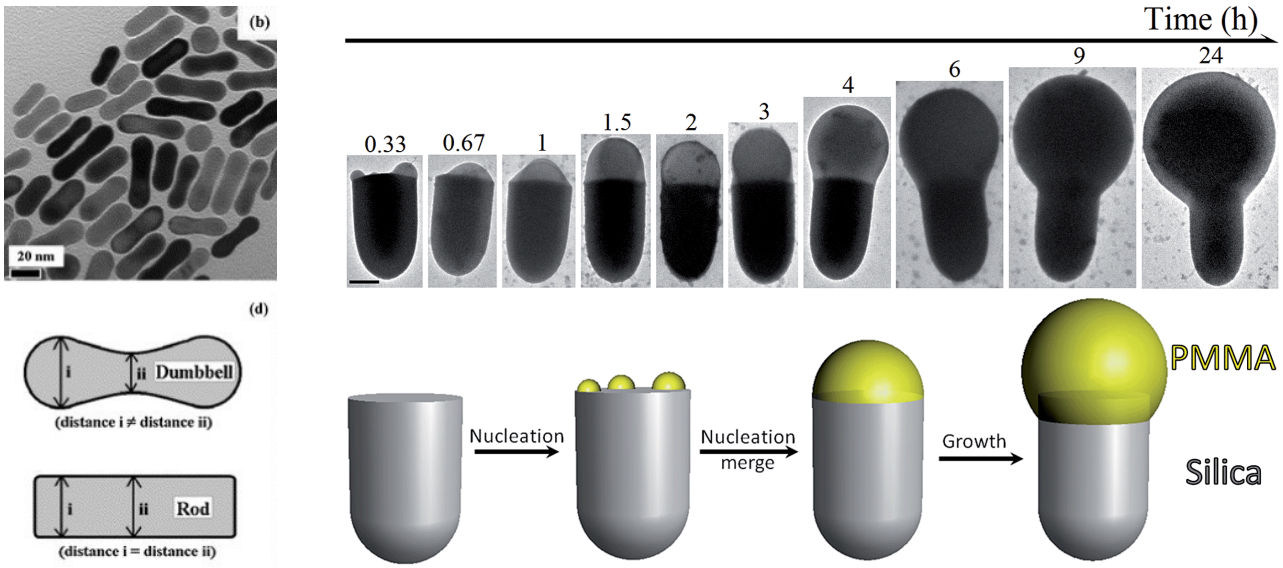

Figure 1.2: Experimental synthesis of dumbbell and lollipop particles. Left: TEM image of gold nanodumbbells (top) and a drawing of its morphology (under) [11]. Right: Interval TEM images of colloidal lollipops (top) and cartoon of the process (under) [12].

2 Methods

2.1 Metropolis Monte Carlo Simulations

To simulate the liquid crystal behavior of elongated hard particles we use the Monte Carlo (MC) method. The MC method is based on random sampling to obtain numerical results. Consider the canonical ensemble where the number of particles N, the volume V and the temperature T are fixed. The Hamiltonian describing this system is given by

$$H(\mathbf{r}^N, \mathbf{p}^N) = \sum_{i=1}^{N} \frac{\mathbf{p}_i^2}{2m} + U(\mathbf{r}^N), \tag{2.1}$$

with the momenta $\mathbf{p}^N$ of the particles and the potential U, depending on the positions $\mathbf{r}^N$ of these particles. For this system the canonical partition function is given by

$$Z(N, V, T) = c \int d\mathbf{r}^N exp(-\beta U(\mathbf{r}^N)), \tag{2.2}$$

where $\beta = 1/k_b T$ with Boltzmann constant k_b and c a normalization constant resulting from integrating over the momenta. We can now express the average of a momentum-independent observable O as

$$\langle O \rangle = \frac{\int d\mathbf{r}^N O(\mathbf{r}^N) exp(-\beta U(\mathbf{r}^N))}{\int d\mathbf{r}^N exp(-\beta U(\mathbf{r}^N))}. \tag{2.3}$$

Because we can not easily calculate the integral over the whole phase space, we use the Monte Carlo method. Instead of integrating over the entire phase space we consider a set of n configurations $\mathbf{r}_1^N, \mathbf{r}_2^N, ..., \mathbf{r}_n^N$. For n random configurations, a Markov chain, the ensemble average would be

$$\langle O \rangle = \frac{\sum_{i=1}^{n} O(\mathbf{r}_i^N) exp(-\beta U(\mathbf{r}_i^N))}{\sum_{i=1}^{n} exp(-\beta U(\mathbf{r}_i^N))}. \tag{2.4}$$

In a Metropolis sampling algorithm [8] we generate $\mathbf{r}_i^N$ so that the probability of generating $\mathbf{r}_i^N$ is proportional to $exp[-\beta U(\mathbf{r}_i^N)]$. The ensemble average reduces to

$$\langle O \rangle = \frac{\sum_{i=1}^{n} O(\mathbf{r}_i^N)}{n}. \tag{2.5}$$

The algorithm starts with an initial configuration $\mathbf{r}_{init}^N$ and computes a trial configuration $\mathbf{r}_{trial}^N$ where, for example, a random particle is moved. The new trial configuration is accepted with probability

$$acc(init \to trial) = min(1, exp\{-\beta[U(\mathbf{r}_{trial}^N) - U(\mathbf{r}_{init}^N)]\}) \tag{2.6}$$

The initial configuration is kept if the move is rejected. By repeating these steps many times the system will reach an equilibrium from which the average observable can be calculated.

2.2 Isobaric-Isothermal Ensemble

In the previous section we described the Metropolis Monte Carlo method in a canonical or NVT ensemble. It is sometimes convenient to fix the pressure P instead of the density, specifying a pressure is usually easier. Therefore, in this thesis, we mainly use the isobaric-isothermal NPT ensemble. In the NPT ensemble additional steps are performed to change the volume V of the system. Trial moves are now accepted with probability

$$acc(init \to trial) = min(1, (V_{trial}/V_{init})^N exp\{-\beta P[V_{trial} - V_{init}] - \beta[U(\mathbf{r}_{trial}^N) - U(\mathbf{r}_{init}^N)]\}). \tag{2.7}$$

To complete our acceptance method we need to define a potential between particles. The potential between a pair of hard particles can be written as,

$$\beta U = \begin{cases} \infty & \text{overlap between particles} \\ 0 & \text{no overlap} \end{cases}. \tag{2.8}$$

Overlap of particles will result in a rejection of the trial configuration. An important part in the simulations is to find a way to check for overlaps between particles. For each different shape an efficient algorithm has to be constructed to find the minimum distance between the particles.

2.3 Periodic Boundary Conditions

In computer simulations very large (infinite) systems can not be easily simulated. We need large systems to reduce the fraction of particles on the surface. For a three-dimensional system the fraction of particles on the surface is about $N^{-1/3}$. Even a system of a million particles has approximately 6% of the particles at the surface. Periodic boundary conditions (PBCs) can be used to approximate large (infinite) systems and avoid surface effects. In Fig. 2.1 we can see that the simulation box is duplicated in all directions. If a particle crosses the boundary of the box it will appear at the other side of the box. This way there are no boundaries at the edges eliminating surface effects. All particles in the box follow the nearest image convention so that each particle always interacts with the nearest image of all other particles. The box size of the system must be large enough so that there is no self-interaction.

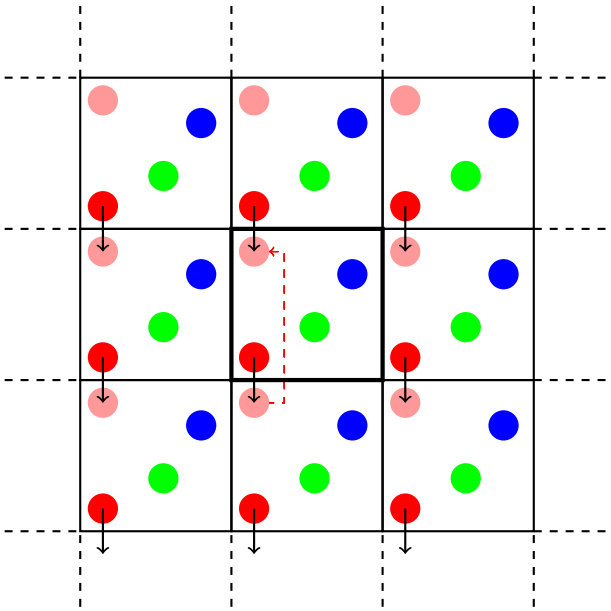

Figure 2.1: Periodic boundary conditions. One central box with duplicates surrounding it. The arrows show a particle move outside the boundary box.

2.4 Cell Linked-List

Reducing computational time has a high priority in simulations. Faster algorithms can therefore simulate larger systems and or perform more steps. Efficient overlap algorithms help to reduce the computational time. Instead of checking if a particle overlaps with all other particles in the system, we can reduce this to the number of particles it can overlap with when moved. We divide the system in a set of cube shaped cells where each cube is large enough to fit the bounding sphere of a particle. Each particle now has its

center in one of these cells. If the maximum displacement of a particle is smaller then the size of a cell we only have to check overlaps with particles in the neighboring cells. When checking for neighboring cells we also have to take into account the periodic boundary conditions. Fig 2.2 shows a 2 dimensional cell grid where circles outside the highlighted orange cells can not overlap with the blue circle. In this example the green circle is just inside a neighboring cell and should be checked for overlap.

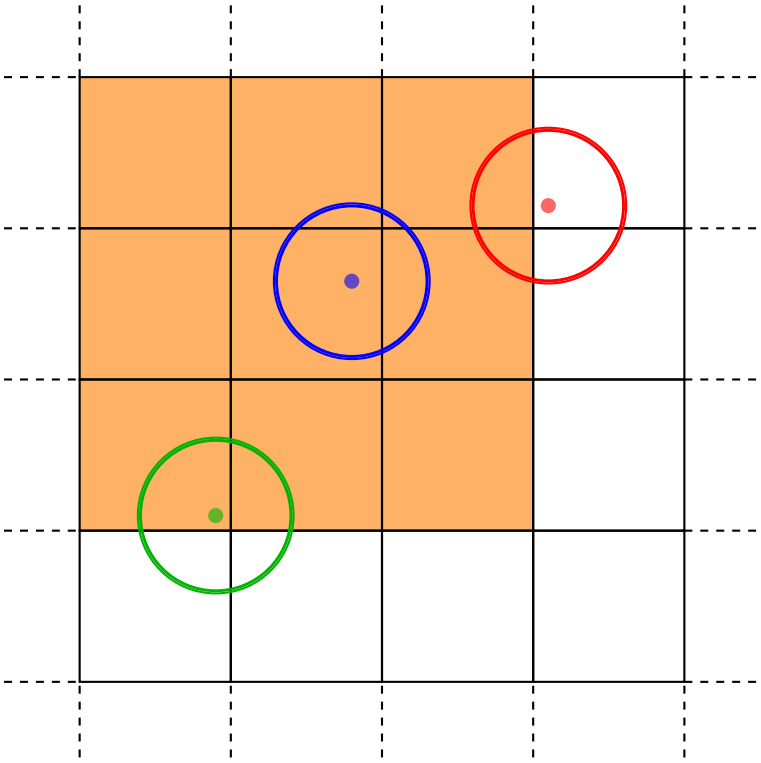

Figure 2.2: 2D Cell list. In a cell list the blue circle will check for overlaps in all orange cells. The red circle has its center outside and the green inside these cells.

Linked List

Keeping track of which particle is in which cell can be an administrative challenge. Here we use a linked list algorithm. An array keeps track of the first particle in each cell. If there are more particles in a cell they are put in a linked array where each particle in the array is linked to the next particle in the list. To illustrate this consider 3 particles (e.g. the number 2, 13 and 52) in cell number 16.

```
Cell[16]=2;
LinkedList[2]=52;
LinkedList[52]=13;
LinkedList[13]=-1;
```

The end of the linked list or an empty cell is set to -1. If a particle moves to another cell the linked list has to be updated without leaving broken chains in the list.

Bounding spheres

For elongated particles the cells could become very large and lose their efficiency. To solve this we wrap the particle in a group of smaller bounding spheres. The bounding spheres completely encapsulate the elongated particle. In Fig. 2.3 we show an example of a spherocylinder and its bounding spheres.

The cells are resized to fit the smaller bounding spheres. The cells, and all their neighboring cells, where the bounding spheres are in should be checked for overlapping particles. A particle can be in multiple cells so we subdivide each particle in the number of bounding spheres. This increases the size of the linked list, $\#\,particles \times \#\,bounding\,spheres$.

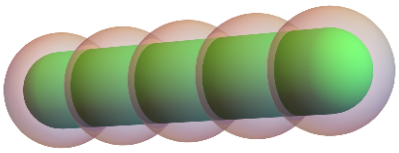

Figure 2.3: Bounding spheres encapsulating a spherocylinder.

2.5 Algorithm overview

Now that we have the basic techniques for a Monte Carlo simulation we describe a main overview of the program in the NPT ensemble.

Algorithm 1 Basic algorithm concept

```
1: while Cycle < MaximumCycles do
2:     while Step < N do
3:         if RandomNumber[0, 1] < 0.5 then TranslationMove
4:         else RotationMove
5:     VolumeMove
```

Simulations start with an initial configuration of N particles. Each particle has a three dimensional position $\mathbf{r}$ and unit vector $\mathbf{u}$ describing its position and orientation. A random particle i is selected and with 50% probability either translated or rotated. For each translation a random dimension is chosen. In this dimension the particle is translated randomly between interval $[-r_{max}, r_{max}]$. For rotations a random unit vector is generated. The particle is rotated randomly in this direction in the interval $[-\theta_{max}, \theta_{max}]$. r_{max} and θ_{max} are rescaled every 100 cycles so that a 30% acceptance rate is achieved. After N steps a volume move is performed. Here the box and all particles are scaled in a random dimension in the interval $[-V_{max}, V_{max}]$. V_{max} is also rescaled every 100 cycles for a 25% acceptance rate. These N steps complete one cycle. For the system to reach equilibrium many cycles need to be performed.

2.6 Computation times

The efficiency of the simulation techniques described in Sec. 2.4 is defined by the average computation time needed for simulating a certain number of Monte Carlo cycles. We perform 1000 Monte Carlo cycles without cell list, with cell list but without bounding spheres, and with a cell list with different bounding sphere diameters. The length of a particle affects the computation times, therefore we simulate hard spherocylinders (model described in Sec. 3.2) with length $L/D = 5$ and $L/D = 9$. For each run, we start with the same number of particles $N = 728$, starting configuration, and pressure. In Fig. 2.4, we plot the computation times for 1000 Monte Carlo cycles for the cases described above. The bounding sphere diameter are $\sigma/D \in [1.1, 1.5]$. Without cell list the computation times for both $L/D = 5$ and $L/D = 9$ are about the same as overlaps between all particles have to be checked. The length of a particle does not affect the efficiency of the overlap algorithm. This is the case for simulations with cell list. For longer particles the size of the cells increase. More particles are stored in each cell resulting in more overlap checks. Dividing the elongated particles in more bounding spheres reduces the computational times significantly. With bounding spheres the simulations are on average five times faster than without cell list. For bounding spheres with smaller diameters the particle is included in more cells. Larger bounding spheres result in larger cell sizes and more particles to check for overlaps. For both $L/D = 5$ and $L/D = 9$ a bounding sphere diameter of $\sigma/D = 1.3$ shows the shortest computation time.

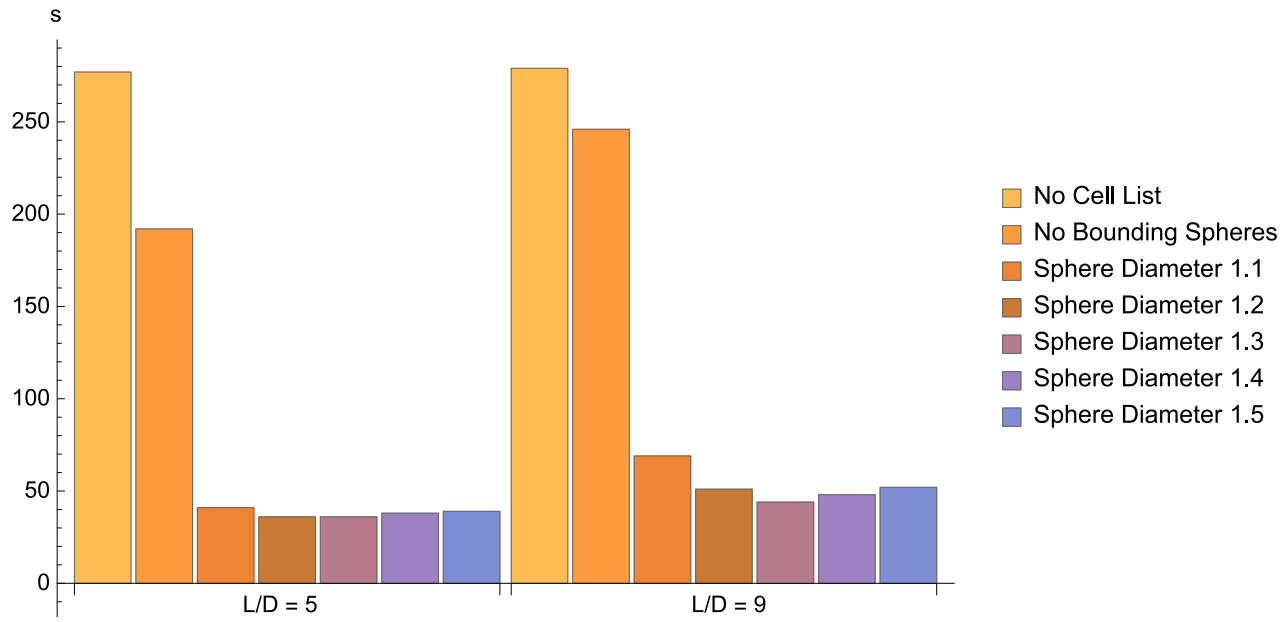

Figure 2.4: Computation times for spherocylinders with length $L/D = 5$ (left) and $L/D = 9$ (right). Colored bars indicate different techniques used to improve the efficiency of the simulations. From left to right we simulate $N = 728$ spherocylinders for 1000 Monte Carlo cycles without cell list, cell list without bounding spheres and bounding spheres with bounding sphere diameter $\sigma/D \in [1.1, 1.5]$.

3 Results

Our main goal for this thesis is to simulate hard elongated dumbbells and lollipops. Before we can provide results on these particles we need to verify the correctness of our simulation methods. Both dumbbells and lollipops are a combination of spheres and spherocylinders. To test our model we should first validate our results for these two well studied shapes.

3.1 Spheres

As we mentioned in the introduction, one of the first studies using computer simulations was the Monte Carlo simulation of hard spheres. This simple model is ideal to start with. In a hard sphere model we define the pair potential as

$$\beta U(r_{ij}) = \begin{cases} \infty & r_{ij} < \sigma \\ 0 & r_{ij} \geqslant \sigma \end{cases}. \tag{3.1}$$

If the distance r_{ij} between the centers of two spheres i and j is smaller than the diameter of a sphere σ they overlap. Overlap results in an infinite pair potential and thus a rejection of the performed move.

3.1.1 Equation of state

Common practice in scientific studies is to use SI units. In the colloidal regime these units would result in very small numbers. Instead we use reduced units. For a system of hard spheres we set the diameter of a sphere as unit length. The size of the system will be in lengths of these units. We use a reduced pressure $P^* = \beta P v_0$ with the volume of a particle v_0 and $\beta = 1/k_B T$, with Boltzmann constant k_B and temperature T. For spheres of diameter σ, $v_0 = 4/3\pi(\sigma/2)^3$. The fraction of the occupied volume in a box of volume V with a number of particles N is defined by the packing fraction

$$\eta = \frac{N v_0}{V}. \tag{3.2}$$

The packing fraction can vary from 0 for an empty box to 1 which is a completely filled box. The equation of state relates the packing fraction of a system to its pressure. At higher pressures the density of the system increases. For spheres the closest packing fraction is the FCC (face centered cubic) crystal with $\eta = 0.74$ at infinite pressure, as shown in Fig. 3.1a. In a fluid phase the spheres lose their order and are free to flow like a liquid. A snapshot of a fluid phase is shown in Fig. 3.1b.

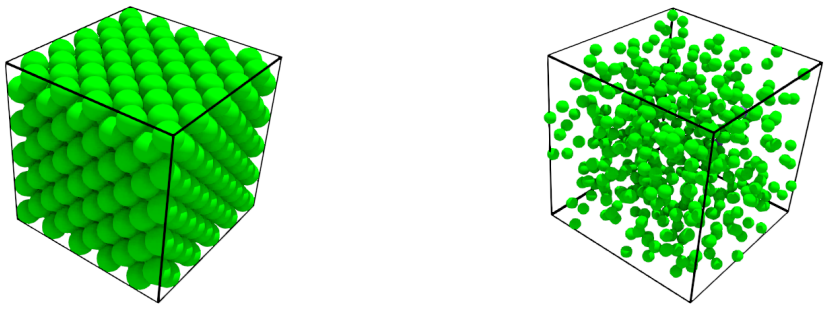

(a) FCC crystal **(b)** Fluid structure

Figure 3.1: Snapshots of an FCC crystal structure with $\eta \approx 0.74$ (a) and a fluid structure with $\eta \approx 0.22$ (b) of N=500 hard spheres

By using computer simulations in the NPT ensemble we can measure the average packing fraction for hard spheres as a function of the compressibility

$$Z = \frac{\beta P V}{N} \tag{3.3}$$

The fcc crystal is chosen as initial configuration. For each fixed pressure we let the system reach an equilibrium state. The average packing fraction for each equilibrated pressure is plotted in Fig. 3.2. For hard spheres in the isotropic liquid phase the equation of state can be approximated by the Carnahan and Starling equation [15]

$$Z = \frac{1 + \eta + \eta^2 - \eta^3}{(1-\eta)^3}. \tag{3.4}$$

In the crystal phase the equation of state can be approximated by the Speedy equation [16]

$$Z = \frac{3}{1-z} - \frac{a(z-b)}{z-c}. \tag{3.5}$$

For the fcc crystal $z = (6\eta)/(\pi\sqrt{2})$, $a = 0.620735$, $b = 0.708194$ and $c = 0.591663$ [17]. The simulated results match the theoretical approximations shown in Fig. 3.2.

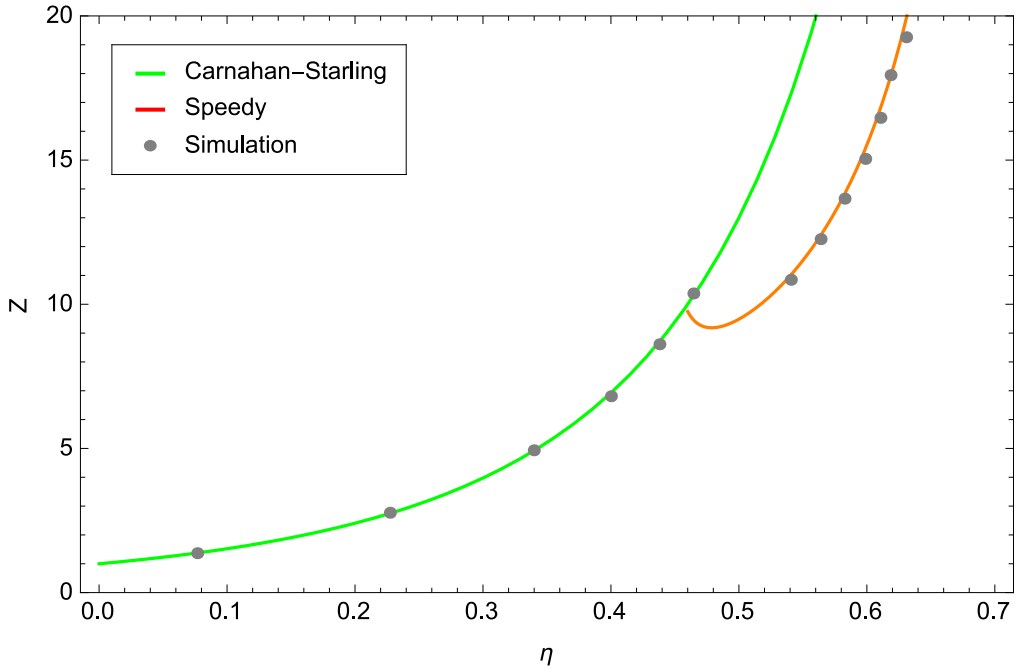

Figure 3.2: Equation of state for hard spheres. Gray dots indicate the simulation results for N=500 spheres. Green and Red lines are the theoretical approximations from Carnahan and Starling (green) and Speedy (red).

3.2 Spherocylinders

In 1949 Onsager predicted an isotropic-nematic transition for a system of hard thin rods [18]. Although the orientational ordering of the system decreases the orientational entropy of the system, Onsager showed that the increase in translational entropy more than compensates for this loss. An increase in order increases the total entropy due to the gain in free volume per particle. After the isotropic-crystal phase transition was shown for hard spheres computer simulations on hard spherocylinders showed, in addition to Onsager's predicted nematic phase, a smectic liquid crystal phase [19]. For the spherocylinders we use the diameter

of the rod D as unit length. The aspect ratio between the length of the rod L and the diameter, L/D, is the only shape parameter. In addition to the position $\mathbf{r}$ these anisotropic particles have a unit vector $\hat{\mathbf{u}}$ for their orientation. The pairwise potential depends on the positions and orientations as

$$\beta U(r_{ij}) = \begin{cases} \infty & d_{ij}(\mathbf{r}_{ij}, \mathbf{u}_i, \mathbf{u}_j) < D \\ 0 & d_{ij}(\mathbf{r}_{ij}, \mathbf{u}_i, \mathbf{u}_j) \geqslant D \end{cases}. \tag{3.6}$$

The minimal distance d between spherocylinders i and j should be larger than its diameter, and can be calculated according to Ref. [20]. The volume v_0 of a spherocylinder is given by

$$v_0 = \frac{\pi}{4} L D^2 + \frac{\pi}{6} D^3. \tag{3.7}$$

3.2.1 Order parameters

To identify the order of each phase we use a set of order parameters. For the hard spheres a jump in the packing fraction determines when the system loses its crystalline order to a fluid phase. In the case of the nematic phase we need to quantify the alignment along the average nematic direction. The global nematic order parameter S is the associated order parameter. S is defined by the maximum eigenvalue of the nematic order parameter tensor

$$Q_{\alpha\beta} = \frac{1}{N} \sum_{i=1}^{N} \left[\frac{3}{2} \mathbf{u}_{i\alpha} \mathbf{u}_{i\beta} - \frac{\delta_{\alpha\beta}}{2} \right]. \tag{3.8}$$

Here α and β indicate a component of orientation $\mathbf{u}$ regarding particle i, N is the number of particles and $\delta_{\alpha\beta}$ the Kronecker delta. The corresponding values for S ranges from 0 for complete isotropic orientation to 1 for perfect orientational alignment. The positional layered ordering in the smectic phase can be calculated with the global smectic order parameter

$$\tau = \max_{l} \left| \sum_{j=1}^{N} e^{2\pi i \mathbf{r}_j \cdot \mathbf{n}/l} \right|, \tag{3.9}$$

where l is the spacing between smectic layers. Low values of τ indicate no smectic ordering. τ will reach values close to 1 when perfect layers of particles are formed.

3.2.2 Simulations

For the simulations on hard spherocylinders we use the approach from McGrother et al. [21]. To test our model we choose $L/D = 5$, the largest aspect ratio presented by McGrother et al. As initial configuration an FCC lattice is scaled in the z-direction by the length of the particles and expanded to a very low packing fraction. For a fixed pressure P^* the system is equilibrated to obtain the average equilibrium packing fraction. The pressure is increased gradually to compress the system from an isotropic phase to the crystal phase. The equation of state is presented in Fig: 3.4a along with the simulation results from McGrother et al. To identify the different phases we use the order parameters as described in Sec. 3.2.1. The nematic and smectic order parameters are shown in Fig. 3.4b. They confirm the different phases identified by McGrother et al. in the equation of state. Snapshots of the different phases are shown in Fig. 3.3.

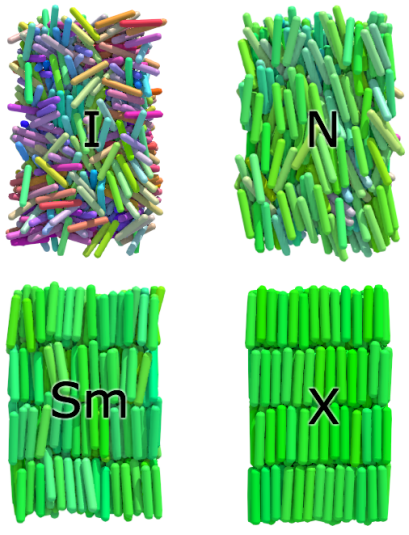

Figure 3.3: Different phases formed by hard spherocylinders. Isotropic (I), nematic (N), smectic (Sm) and crystal phase (X).

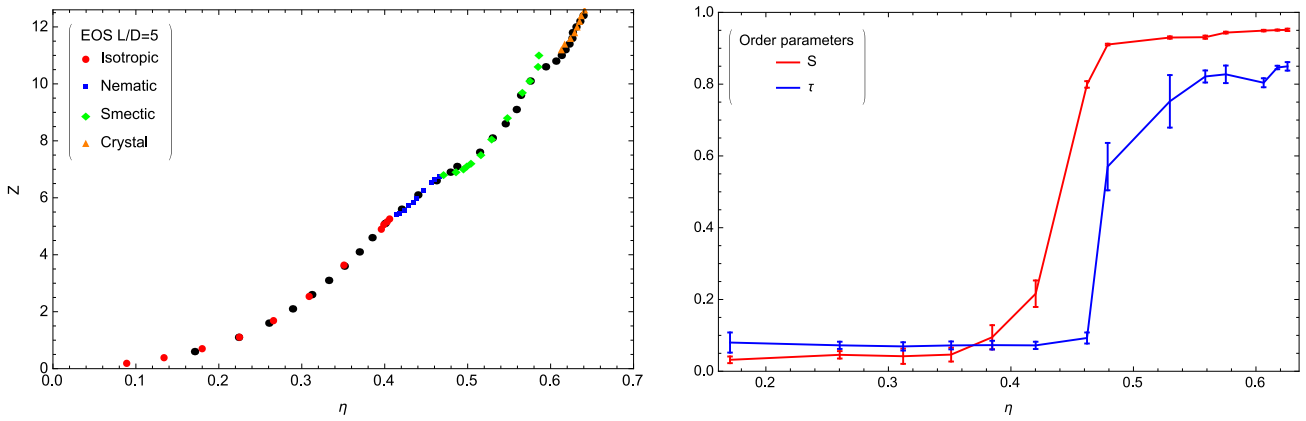

(a) Equation of state **(b)** Order parameters

Figure 3.4: Equation of state (EOS (a)) where the colored points indicate the different phases identified by McGrother et al. [21]. Black points are obtained from simulations of the present work for hard spherocylinders with $L/D = 5$ compressed from an isotropic phase. The order parameters (b) confirm the phases identified in the EOS.

3.2.3 Phase diagram

A detailed study on hard spherocylinders can provide a reference point for the simulations on hard dumbbells and lollipops. In a phase diagram an overview of the different phases is plotted. The highest and lowest packing fraction of each phase is plotted for a range of aspect ratios. In Fig. 3.5 the phase diagram for hard spherocylinders with $3 \leqslant L/D \leqslant 7$ is plotted. For low packing fractions the system is isotropic. At higher packing fractions the phase behavior depends on the aspect ratio of the particles. For $L/D \geqslant 3.2$ a smectic phase appears between the isotropic and crystal phase. The isotropic-nematic transition occurs for $L/D \geqslant 4$. For hard spherocylinders there are two types of crystals phases [10]. The closed packed ABC crystal and a AAA crystal (shown in Fig. 3.5) which, for $L/D \geqslant 7$ appears before the ABC crystal.

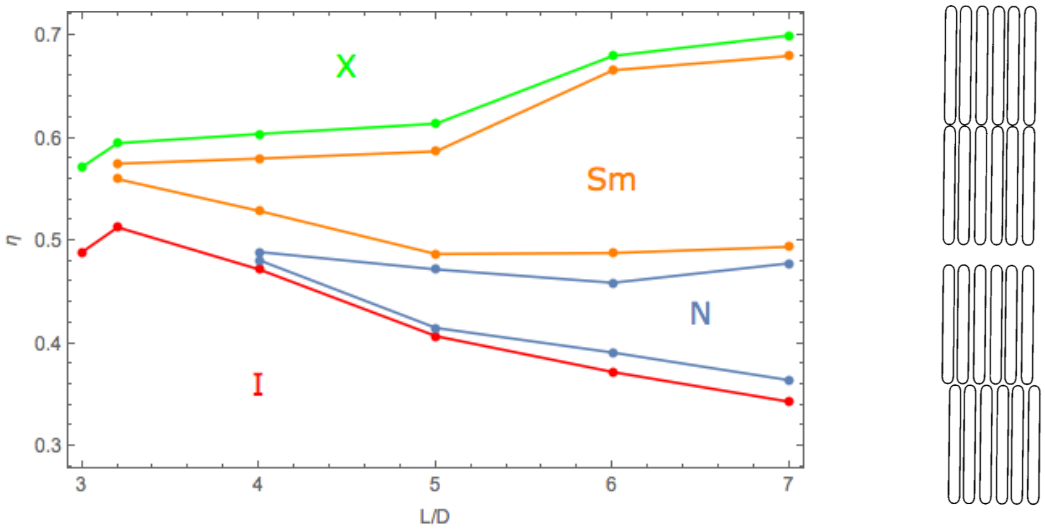

Figure 3.5: Phase diagram for hard spherocylinders. Data based on [21] and extended for aspect ratio $L/D > 5$ with simulation results of the present work. Points denote the limits of the isotropic (I), nematic (N), smectic (Sm) and crystal phase (X) for different aspect ratios L/D. Crystal configurations shown with AAA-crystal (top right) and ABC-crystal (bottom right) adapted from [10].

3.3 Dumbbells

Recent developments in the synthesis of colloidal particles allow experimentalists to study the phase behavior for a variety of colloids and nanoparticles. The synthesis of dumbbell-like structures [11] demands a detailed study of the behavior of these systems. To guide experimentalists in their research we use computer simulations to provided an approximation of the behavior of these elongated dumbbells. The study of elongated dumbbells is quite rare in literature.

A study by de las Heras et al. [13] provides a phase diagram for a system of hard top-shaped particles. These top-shaped particles are modeled as a hard sperocylinder, like the dumbbells, but with a single hard sphere in its center. De las Heras et al. report, beside the nematic and smectic liquid crystal phases, the stability of the columnar phase. In this thesis we want to use the information from the top-shaped particles to present phase diagrams for the hard dumbbells and see if they can self-assemble into a columnar phase.

Back in 1995, de Gennes suggested in his book on liquid crystals [14] a cholesteric nematic phase for dumbbell-like particles. In Fig. 3.6 de Gennes explains how this differs from an achiral nematic phase in terms of minima in the free energy F as a function of the twist q. The minimum in free energy for the cholesteric phase occurs at $q \neq 0$. In case of hard dumbbells a spontaneous symmetry breaking is expected and the free energy should have two minima at $\pm q^* \neq 0$. According to de Gennes no helices of this kind have been found in liquid crystals yet but short range helices have been observed in columnar phases. For the hard elongated dumbbells we will study this cholesteric nematic phase suggested by de Gennes.

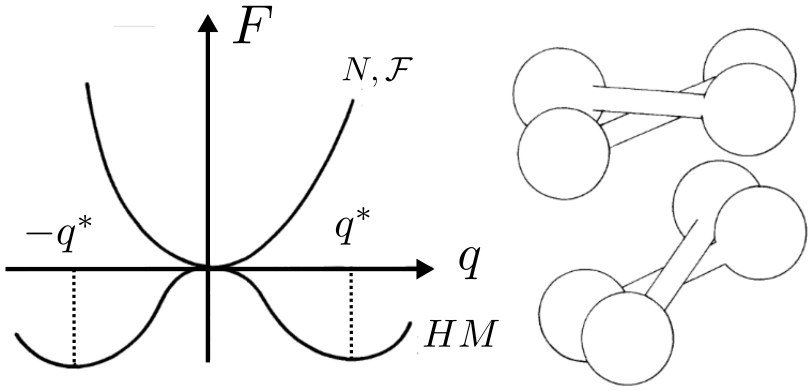

Figure 3.6: Adapted from Ref. [14] with original caption: Variation of the free energy with twist. The curve labeled N, F applies to a nematic or a ferromagnet (minimum of energy at zero twist). The curve labeled HM applies to a helimagnet, or to the dumbbels of the inset.

3.3.1 Model and methods

We model the dumbbell particle as a hard spherocylinder with two hard spheres at each end as shown in Fig. 3.7. The spherocylinder, as described in Sec. 3.2, has length L and diameter D. The two spheres each have the same diameter σ. The diameter of the sphere is larger than that of the cylinder $\sigma > D$. The dumbbells only interact via hard-body interactions. All pairwise overlaps, such as spherocylinder-spherocylinder, sphere-spherocylinder and sphere-sphere are forbidden. The volume of a dumbbell in our model consists of the volume of a central cylinder and the volume of the two partial spheres on each end. For an exact volume of the particle we first calculate the volume of the partial spheres at each end. The volume of a spherical cap is given by

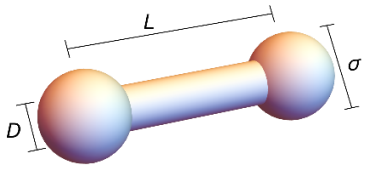

Figure 3.7: Graphical representation of a dumbbell with cylinder length L, cylinder diameter D and sphere diameter σ.

$$V_{cap} = \frac{1}{6}\pi h(3\frac{D}{2}^2 + h^2), \tag{3.10}$$

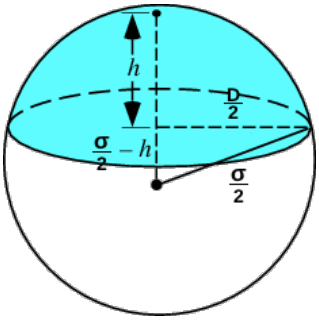

Figure 3.8: Graphical representation of a spherical cap, with the height of the cap h, radius of the cylinder $\frac{D}{2}$ and radius of the spheres $\frac{\sigma}{2}$.

where h the height of the cap as dispicted in Fig. 3.8. The volume of the partial sphere at each end of the cylinder is $V_s = \frac{3}{4}\pi(\frac{\sigma}{2})^3 - V_{cap}$. The volume of the central cylinder is $V_c = \pi[L - 2(\frac{\sigma}{2} - h)](\frac{D}{2})^2$. This results in a total volume for a dumbbell

$$V_{sc} = 2V_s + V_c. \tag{3.11}$$

We perform Monte Carlo simulations in the NPT ensemble to study the phase behavior of the hard dumbbells. The size of the system is N=728 particles. The initial configuration is a close packed hexagonal AAA-crystal with 4 layers oriented along the long side of the particles. The box size in the other dimensions is larger than the length of a particle to prevent self interaction. We choose the diameter of the cylinder as constant unit length D=1 and vary the length of the cylinder and diameter of the spheres. For each pressure $P^* \in [2, 20]$ we perform $5{\cdot}10^6$ Monte Carlo cycles.

3.3.2 Results

De las Heras et al. [13] presented a phase diagram of top-shaped particles with aspect ratio $L/D = 5, 9, 13$ and 17. For $L/D = 9$ a nematic, smectic and columnar phase were found. We start our study on hard dumbbells with this aspect ratio and vary the sphere diameter for $\sigma/D \in [1, 1.7]$, where $\sigma/D = 1$ is a spherocylinder. In Fig. 3.10 we present the order parameters and equations of state for $\sigma/D = 1.1, 1.3, 1.5$ and 1.7. For $\sigma/D = 1.1$ we can identify four different phases. At low packing fractions the system is isotropic, both the nematic and smectic order parameters are low. The isotropic-nematic transition is identified by the jump in the nematic order parameter S. The transition from the nematic to the smectic phase is visible from the increase in smectic order τ. Both these transitions are not clearly visible from the equation of state, there is only a small jump in packing fraction η at the corresponding transitions. At the smectic-columnar transition we observe a clear jump in η. For the columnar phase, S approaches 1 and τ strongly decreases. In the nematic and smectic phase, the long axes of the particle $\hat{\mathbf{u}}$ has long range orientational order. In the columnar phase, the particles align in a hexagonal two dimensional lattice but flow freely along the average direction associated to $\hat{\mathbf{u}}$. Visual inspection of the configurations, as shown in Fig. 3.9, confirm this analysis. Further inspection of Fig. 3.10 shows for $\sigma/D > 1.3$ that the smectic phase disappears. The nematic-columnar transition is clearly visible in the equation of state with an increase in η. Beyond this aspect ratio the isotropic phase jumps directly to the columnar phase. Clearly visible in the equation of state and nematic order. We combine the simulation results for sphere diameters $\sigma/D \in [1, 1.7]$ in a phase diagram for hard dumbbells with $L/D = 9$ in Fig. 3.11.

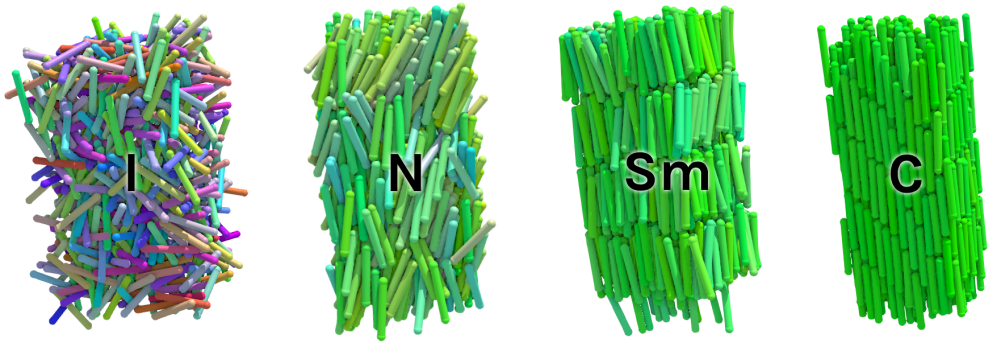

Figure 3.9: Snapshots of dumbbell configurations in the isotropic (I), nematic (N), smectic (Sm) and columnar phase (C). Coloring of the particles according to the orientation of their long axes.

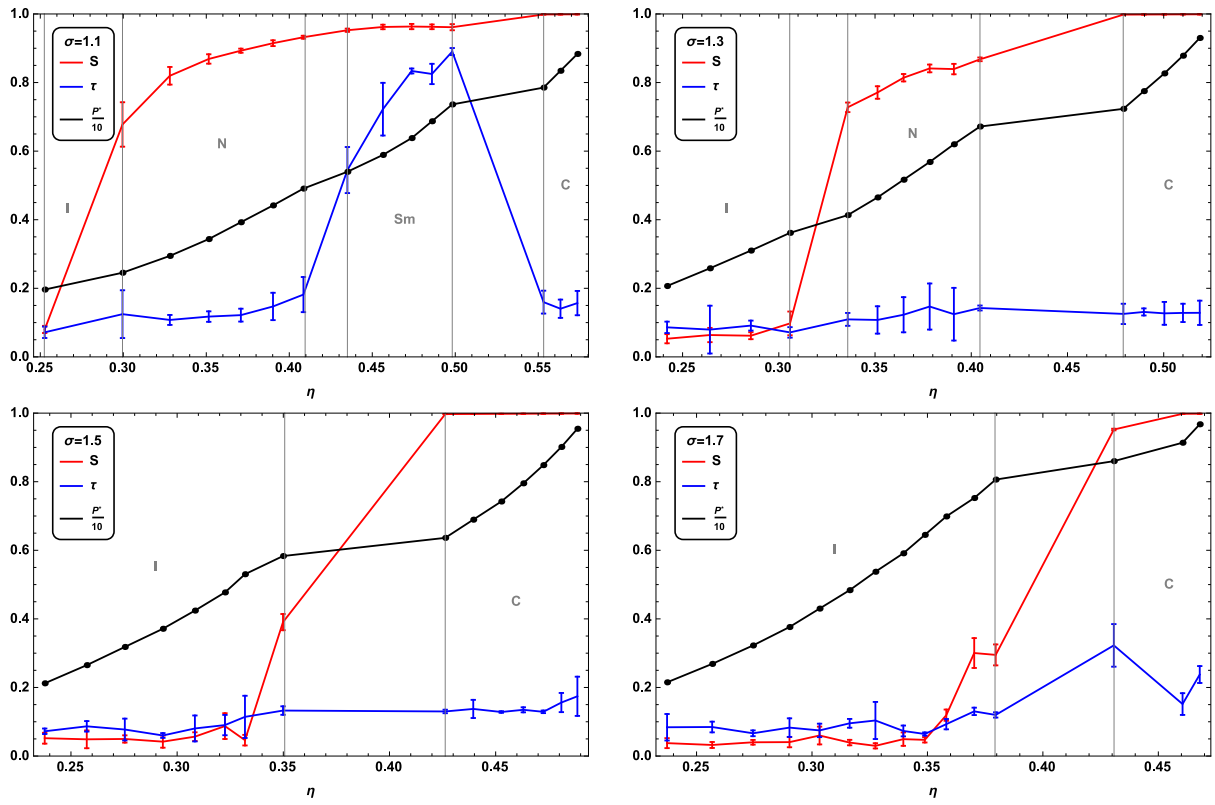

Figure 3.10: Nematic order parameter S, smectic order parameter τ and reduced pressure P^* versus the packing fraction η for dumbbells with length $L = 9$ and sphere diameter $\sigma = 1.1$ top left, $\sigma = 1.3$ top right, $\sigma = 1.5$ bottom left and $\sigma = 1.7$ bottom right. Points are joined by lines for guidance.

The phase diagram provides insight on the effect of the spheres at each end of the spherocylinder. Each phase transition is affected by the increase in diameter σ/D of the spheres. An increase in σ/D reduces the entropy gained by orientational ordering which destabilizes the nematic phase with respect to the isotropic phase. In the smectic phase the increase of σ/D reduces the free space for the particles within the layers. In the smectic layers the spheres align in the plane of the layers leaving more room between the particles. This reduction in packing fraction destabilizes the smectic phase with respect to the columnar phase. The increase in packing fraction for in-plane structures explains the stabilization of the columnar phase. The system will favor sphere-cylinder pairs over sphere-sphere pairs for smaller packing fractions. For $\sigma/D > 1.2$ the smectic phase disappears leaving a nematic-columnar transition. The columnar phase is destabilized for $\sigma/D > 1.5$ due to an increase in space between columns. In Fig. 3.12 we present the phase diagram for $L/D = 7$. As expected from the results for the spherocylinders, a smaller aspect ratio L/D decreases the range of the nematic and smectic phases. For $L/D < 5$ (phase diagram not shown here) the smectic phase completely disappears which differs from the spherocylinders where the nematic phase disappears before the smectic phase. The destabilization of the columnar phase, due to an increase in space between columns, at $\sigma/D > 1.5$ occurs for $L/D = 5, 7$ and 9. In the simulations on $\sigma/D = 1.0$ or spherocylinder, a columnar phase is observed. The stability of the columnar phase for hard spherocylinders is rare in literature. Frenkel et al. [22] describe a columnar phase in small systems of $N = 90$ particles and a $L/D < 5$. According to Frenkel et al. the stability of the columnar phase is due to the finite system size and boundary conditions which allows columns to slide as a whole. An increase in system size $N = 1080$ shifts the columnar phase to an ABC-crystal phase. Simulations of present work show that spherocylinders with ABC or AAA-crystal initial configuration will expand to a columnar phase for a system size $N = 728$ and $L/D > 6$. A decrease in L/D shifts the columnar phase to an ABC-crystal phase. To test the prediction by Frenkel et al. we increase the size of the system to $N = 1740$ and observe that

the columnar phase becomes an ABC-crystal phase for $L/D < 9$. This supports the fact that a columnar phase occurs due to finite system sizes. On the other hand, for a sufficiently large σ the observation of a columnar phase should be a true effect, as it is still observed by an increase in system size.

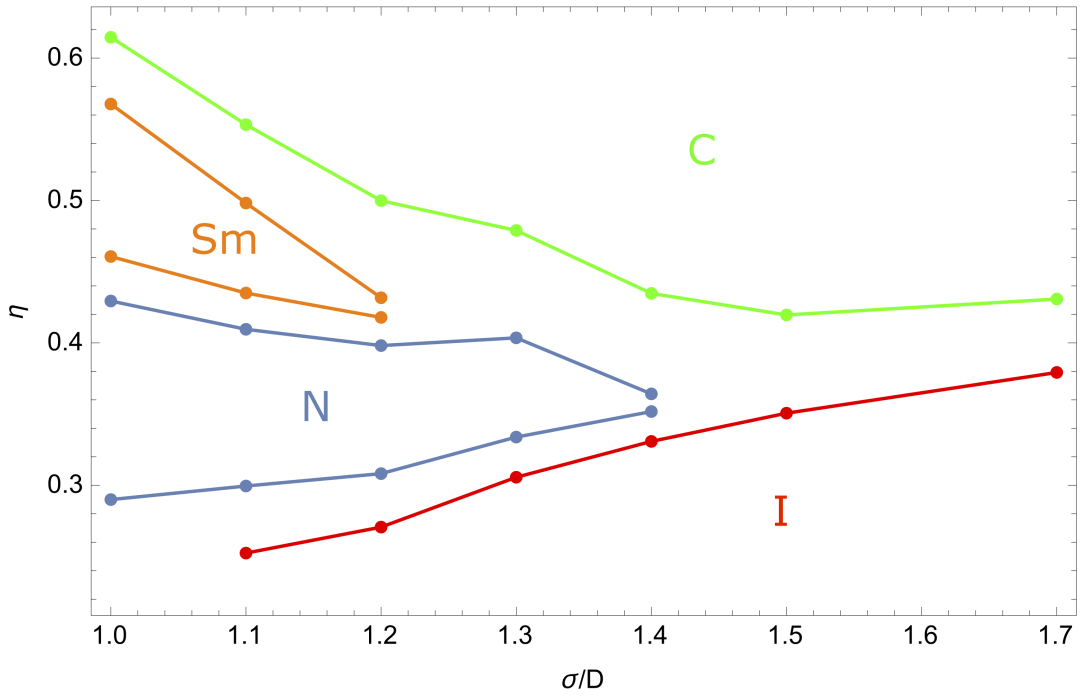

Figure 3.11: Phase diagram for hard dumbbells with $L/D = 9$. Points indicate the boundaries of the phases. Regions include the isotropic (I), nematic (N), smectic (Sm) and columnar (C) phase.

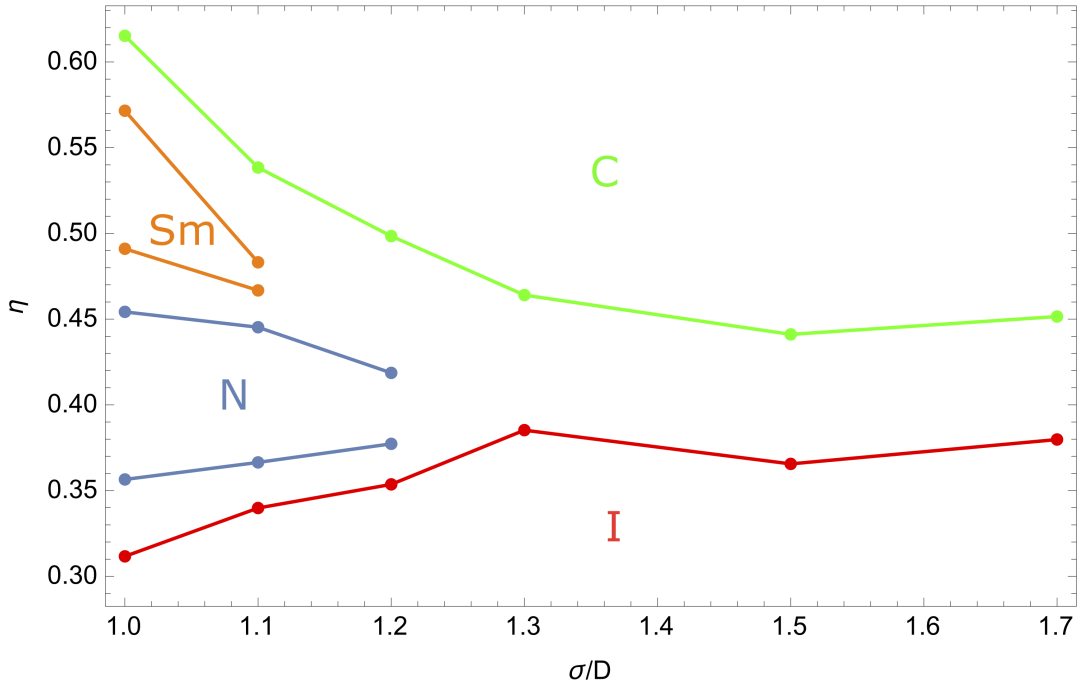

Figure 3.12: Phase diagram for hard dumbbells with $L/D = 7$. Points indicate the boundaries of the phases. Regions include the isotropic (I), nematic (N), smectic (Sm) and columnar (C) phase.

3.3.3 Cholesteric phase

In the previous section we showed that expansion from an ABC or AAA-crystal phase for both dumbbells and spherocylinders can form a columnar phase. Compression runs of spherocylinders did not show a columnar phase. For the dumbbells we can simulate a compression to a columnar phase from an isotropic, nematic or a smectic phase. In the nematic phase the particles are already aligned in the direction of the long axes and have no positional order in this direction. To test if we can compress from a nematic phase into a columnar phase we need to be close to the nematic-columnar transition in the phase diagram Fig. 3.11. For $L/D = 9$ and $\sigma/D = 1.3$ a nematic-columnar transition occurs around $\eta \approx 0.45$. We use a configuration from the edge of the nematic phase and slowly compress the system increasing the pressure by $\Delta P^* = 0.2$ per 10^6 cycles. In Fig. 3.13 we can observe that the system forms short range columns of helices. De Gennes mentions these helices in the columnar phase in his book on liquid crystals [14]. Although the cholesteric nematic phase for dumbbell-like particles has not yet been found, Fig. 3.13 suggests that the system might favor such a phase.

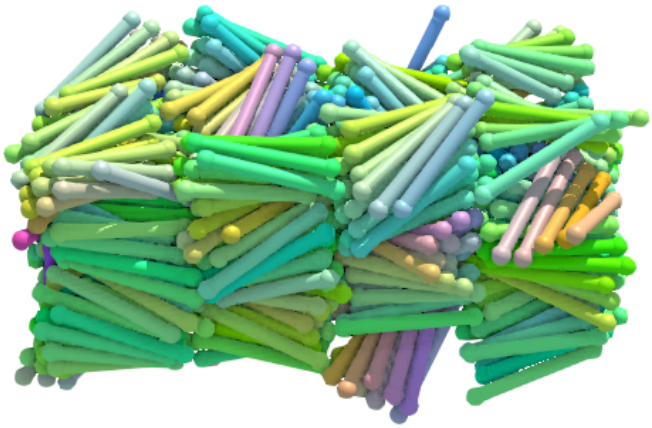

Figure 3.13: Snapshot of hard dumbbells $L/D = 9$ and $\sigma/D = 1.3$ compressed from a nematic phase. Short range columns of helices are formed. Packing fraction of configuration is $\eta \approx 0.51$.

We can force the system in a cholesteric phase by adding a global helical potential. The potential energy with cholesteric pitch q and initial potential U_0 can be writen as

$$U = U_0 \left[\hat{u}_x Cos\left(q\frac{2\pi}{D} z \right) - \hat{u}_y Sin\left(q\frac{2\pi}{D} z \right) \right]. \tag{3.12}$$

Here $\hat{u}_{x,y}$ are the unit vector components in the x, y-direction and $D = 1$ the unit sphere diameter. The potential forces the particles in a helical order around the z-axes. As the initial configuration we choose a close packed honeycomb AAA-crystal. A snapshot of the initial configuration is shown in Fig. 3.14. The size of the system is $N = 3840$ particles. Because we are looking for a nematic cholesteric phase we set the pressure to be in the nematic range. The pitch of the system is set to $q0{=}q/L_z{=}0.25$ and $q_0{=}0.50$ where L_z is the length of the box in the z-direction. On both ends of the box in the z-direction we place walls and turn off its periodic boundary conditions. Particles at the edge of the box are not affected by the rotation of the particles at the other side of the box. The walls limit the translational and rotational freedom of the particles, enhancing the probability for the system to stay in the cholesteric phase. We simulate the system with the potential turned on until the system reaches equilibrium. Snapshots of the final configuration with the potential turned on for both pitches are shown in Fig. 3.14.

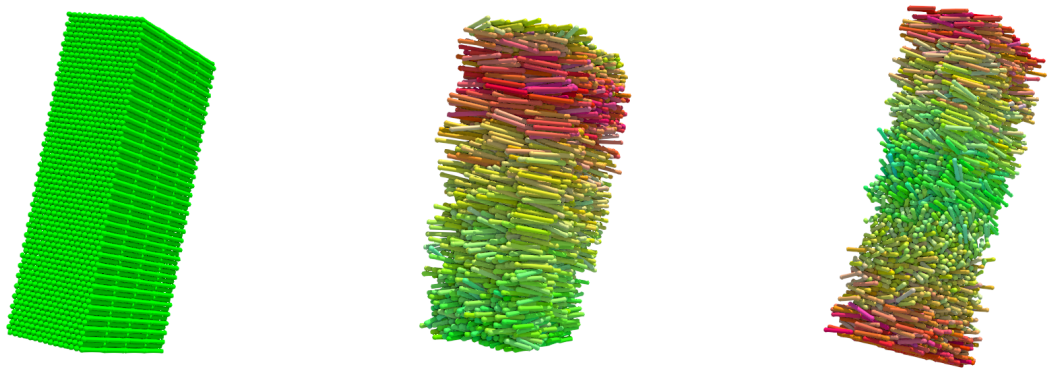

Figure 3.14: Snapshots of the initial configuration (left), configuration with potential turned on and pitch $q = 3.3 \cdot 10^{-3}$ (middle with $q_0 = 0.25$) and $q = 5.8 \cdot 10^{-3}$ (right with $q_0 = 0.50$) for dumbbells with $L/D = 9$ and $\sigma/D = 1.2$. Colors indicate the orientation of the particles.

To calculate the pitch and chirality of the system we use orientational pair-correlation functions that are calculated along the chiral director.

$$S_{220}(z) = \left\langle \frac{3}{2}(\hat{\mathbf{u}}_i \cdot \hat{\mathbf{u}}_j)^2 - \frac{1}{2} \right\rangle \tag{3.13}$$

describes the average nematic order between particle i and j. S_{220} is binned per separation distance z_{ij} over all the particles. If two particles at distance z are perfectly aligned $S_{220} = 1$, while for particles with perpendicular orientations $S_{220} = -0.5$. The chiral organization between particle i and j can be calculated along the z-axes by

$$S_{221}(z) = \langle [(\hat{\mathbf{u}}_i \times \hat{\mathbf{u}}_j) \cdot \hat{\mathbf{z}}_{ij}] \, (\hat{\mathbf{u}}_i \cdot \hat{\mathbf{u}}_j) \rangle \tag{3.14}$$

For the equilibrated configurations in Fig. 3.14, with the chiral potential, the orientational pair-correlation functions are plotted in Fig. 3.15. For both $q_0 = 0.25$ and $q_0 = 0.50$ we can observe that for short ranges the particles align along a common director. For $q_0 = 0.50$, particles that are separated by half the box length are perpendicular to each other. This should be expected for particles separated by a full box length with $q_0 = 0.25$. In the snapshot of the configuration Fig. 3.14 (middle) we can observe that the particles at the top of the box are not increasingly more red as expected. The orientational pair-correlation functions Fig. 3.15 confirm this observation. The wall at the edge of the box confines the particles limiting their movement and therefore preventing the system to order in perfect cholesteric alignment. For $q_0 = 0.50$ the walls do not effect the cholesteric ordering.

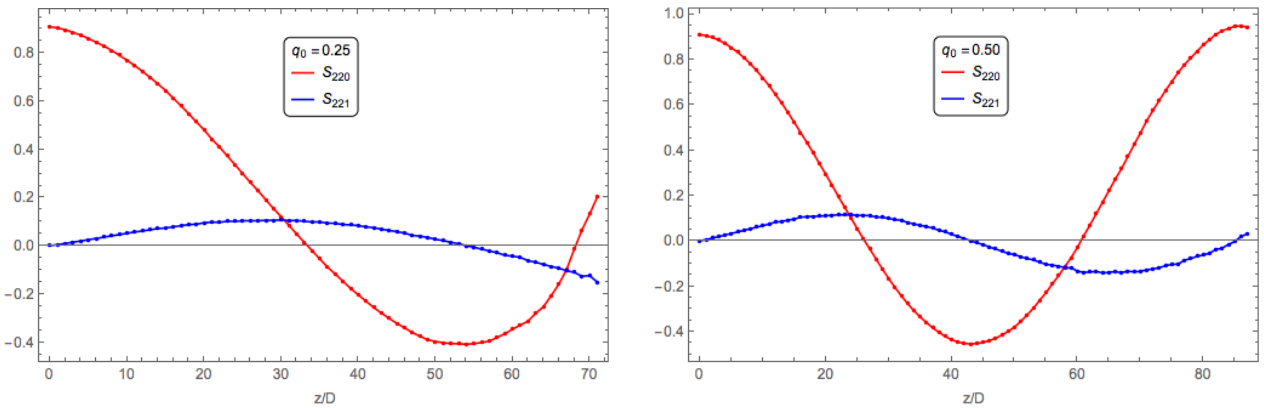

Figure 3.15: Orientational pair-correlation functions S_{220} and S_{221} for hard dumbbell configuration with chiral potential turned on. Plots show pitch $q \approx 3.3{\cdot}10^{-3}$ or $q_0 = 0.25$ (left) and $q \approx 5.8{\cdot}10^{-3}$ or $q_0 = 0.50$ (right).

Now that we have confirmed that the configurations are in a helical cholesteric structure we turn off the potential. We perform Monte Carlo simulations in the NVT-ensemble, where the density of the system stays constant at the edge of the nematic range, $\eta \approx 0.41$ for both $q_0 = 0.25$ and $q_0 = 0.50$. The orientational pair-correlation functions are plotted for the configuration after $2.5 \cdot 10^6$ and $5 \cdot 10^6$ Monte Carlo cycles in Fig. 3.16. The pair correlation functions for configurations shown in Fig. 3.15 are added for comparison. For the system with initial pitch $q_0 = 0.25$ it is hard to tell if the particles are in equilibrium after $5 \cdot 10^6$ cycles. From the configuration after $2.5 \cdot 10^6$ cycles we can observe a lower chiral order pitch. Particles at the edges of the box show a more perpendicular order. Comparison of the correlation function S_{220} after $2.5 \cdot 10^6$ and $5 \cdot 10^6$ show little change in chirality. A small decrease in chiral organization S_{221} suggests that the system is not in an equilibrated cholesteric phase. Confinement of the walls explains the larger difference in S_{220} and S_{221} for particles-pairs at opposite edges. Longer simulations could tell us if the chirality slowly disappears or if the system stays in equilibrium. For the system with $q_0 = 0.50$ a clear decay in chirality is observed. Both correlation functions confirm this decay. At short separation distances z the particles stay aligned to a common director, which is expected in the nematic phase.

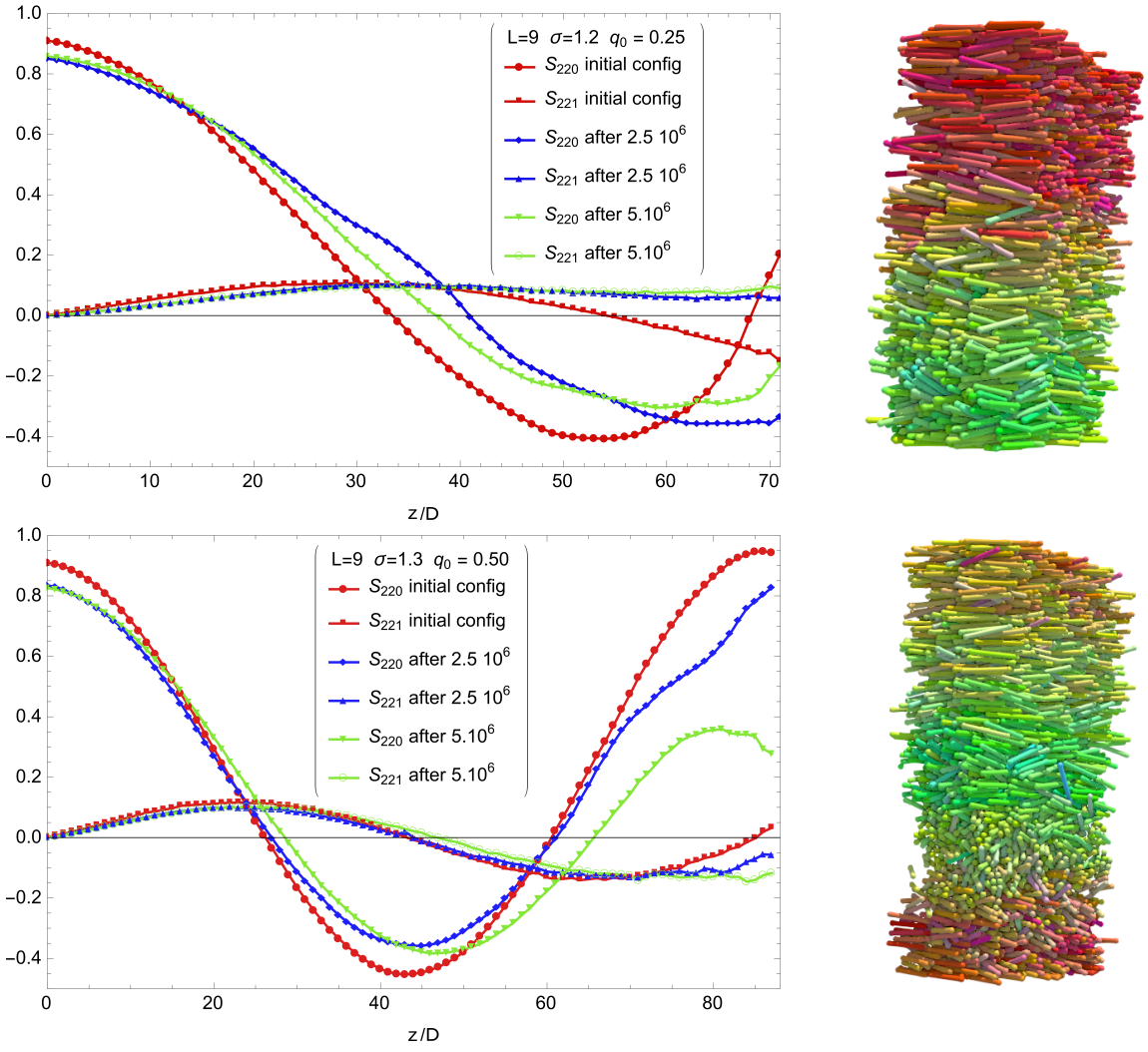

Figure 3.16: Orientational pair-correlation functions $S_{220}(z)$ and $S_{221}(z)$ for hard dumbbells with $L/D = 9$ and $\sigma/D = 1.2$. Correlation functions with initial pitch $q_0 = 0.25$ (top left) and $q_0 = 0.50$ (bottom left) are shown for the initial configuration, after $2.5 \cdot 10^6$ and $5 \cdot 10^6$ Monte Carlo cycles in the NVT-ensemble with packing fraction $\eta \approx 0.41$. Points are joined by lines to guide the eye. Snapshots of the final configurations are shown next to the correlation functions.

In Fig. 3.17 we present the orientational pair-correlation functions for hard dumbbells with $L/D = 9$ and initial pitch $q_0 = 0.25$ for different sphere diameters σ. After turning off the potential and running the simulations in the NVT-ensemble the packing fraction stays constant, $\eta \approx 0.40$ for $\sigma/D = 1.1$, $\eta \approx 0.38$ for $\sigma/D = 1.3$ and $\eta \approx 0.44$ for $\sigma/D = 1.0$ or spherocylinder. For dumbbells with $\sigma/D = 1.1$ the correlation functions do not provide clear evidence for decrease in the chiral order. A snapshot of a configuration after $5 \cdot 10^6$ cycles, Fig. 3.18b shows the chiral order is not significantly decreased. For the spherocylinders, i.e. $\sigma/D = 1.0$, we observe in Fig. 3.18a that the system, after $5 \cdot 10^6$ cycles still shows some chiral order. As we do not expect a cholesteric nematic phase for spherocylinders, longer simulations are needed to equilibrate the system. An increase in sphere diameter from $\sigma/D = 1.1$ to $\sigma/D = 1.3$ decreases the chiral organization, shown in Fig. 3.17. This can also be observed in Fig. 3.18b and 3.18c.

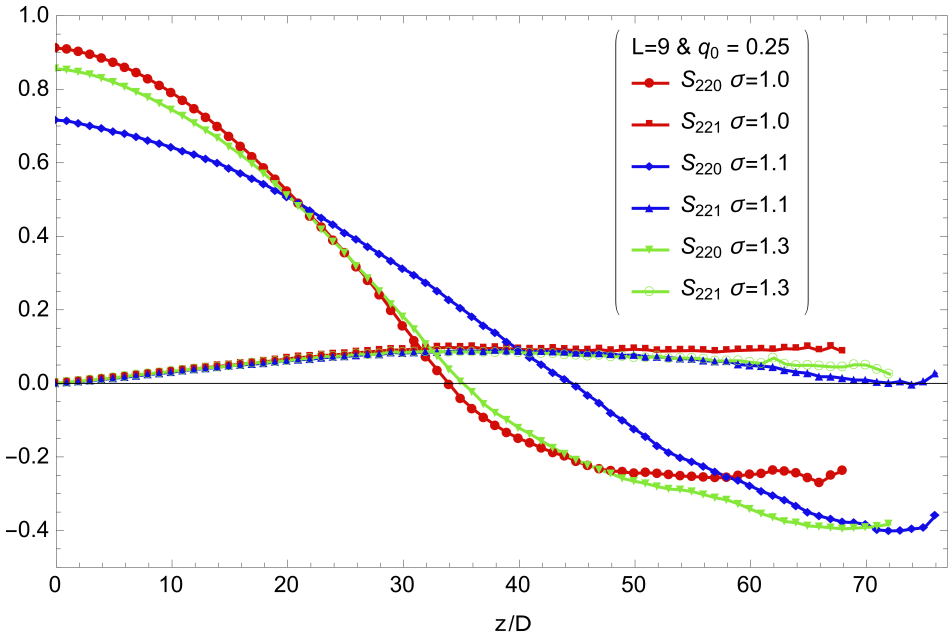

Figure 3.17: Orientational pair-correlation functions S_{220} and S_{221} for hard dumbbells with $L/D = 9$ and $\sigma/D = 1.0$, 1.1 and 1.3 after $5 \cdot 10^6$ Monte Carlo cycles in the NVT-ensemble. Initial pitch of the system $q_0 = 0.25$ or $q \approx 3.6 \cdot 10^{-3}$ for $\sigma/D = 1.0$, $q \approx 3.3 \cdot 10^{-3}$ for $\sigma/D = 1.1$ and $q \approx 3.2 \cdot 10^{-3}$ for $\sigma/D = 1.3$. Points are joined by lines to guide the eye.

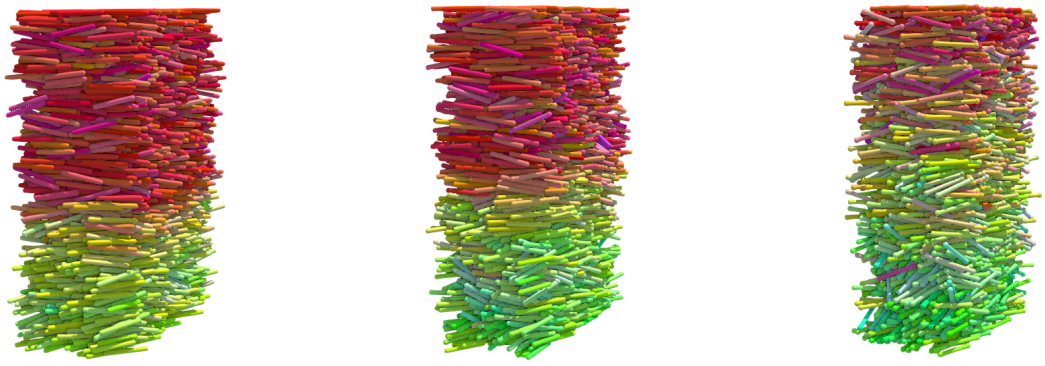

(a) $\sigma/D = 1.0$ & $\eta \approx 0.40$ **(b)** $\sigma/D = 1.1$ & $\eta \approx 0.38$ **(c)** $\sigma/D = 1.3$ & $\eta \approx 0.44$

Figure 3.18: Snapshots of hard dumbbells with $L/D = 9$ and initial pitch $q_0 = 0.25$ after $5 \cdot 10^6$ Monte Carlo cycles in the NVT-ensemble.

A decrease in dumbbell length equilibrates to an achiral nematic order much faster as seen in Fig. 3.19 for dumbbells with $L/D = 7$. The packing fraction $\eta \approx 0.40$ for $\sigma/D = 1.2$ is in the nematic range and $\eta \approx 0.38$ for $\sigma/D = 1.3$ is in the isotropic range. The order parameters show that little chiral order is left for $\sigma/D = 1.2$ whereas for $\sigma/D = 1.3$ the system is completely isotropic. Snapshots of the configurations after $5 \cdot 10^6$ cycles are shown in Fig. 3.20

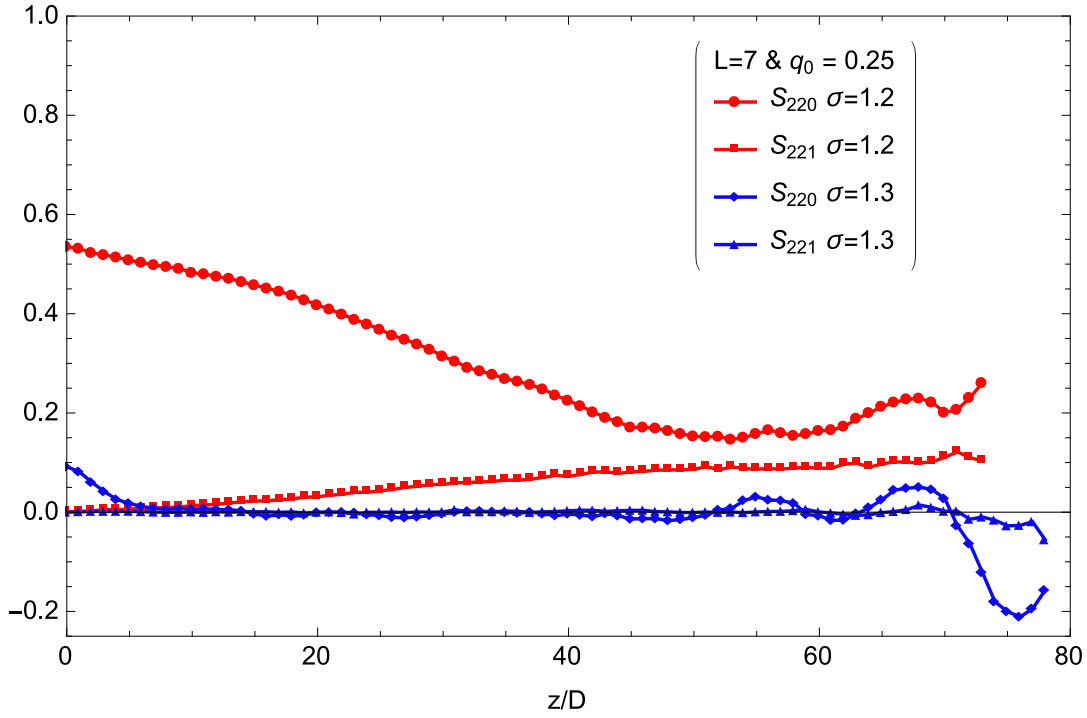

Figure 3.19: Orientational pair-correlation functions S_{220} and S_{221} for hard dumbbells with $L/D = 7$ and $\sigma/D = 1.2$ and 1.3 after $5{\cdot}10^6$ Monte Carlo cycles in the NVT-ensemble. Initial pitch of the system $q_0 = 0.25$ or $q \approx 3.3{\cdot}10^{-3}$ for $\sigma/D = 1.2$ and $q \approx 3.1{\cdot}10^{-3}$ for $\sigma/D = 1.3$. Points are joined by lines to guide the eye.

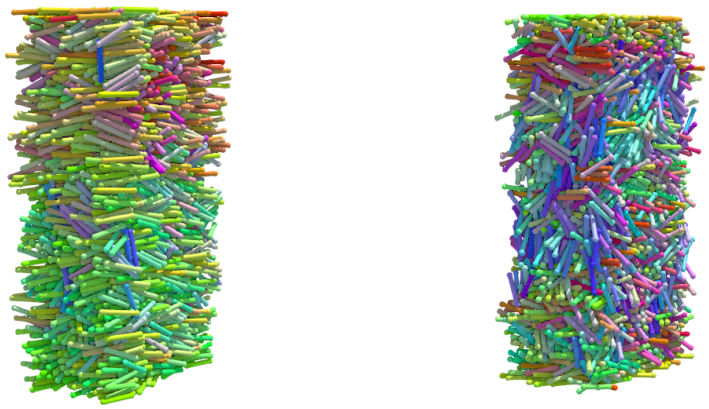

(a) $\sigma/D = 1.2$ & $\eta \approx 0.40$ **(b)** $\sigma/D = 1.3$ & $\eta \approx 0.38$

Figure 3.20: Snapshots of hard dumbbells with $L/D = 7$ and initial pitch $q_0 = 0.25$ after $5 \cdot 10^6$ Monte Carlo cycles in the NVT-ensemble.

3.4 Lollipops

In Sec. 3.3 we presented phase diagrams for hard elongated dumbbells. A study by de las Heras et al. [13] showed the possibility for a stable columnar phase with top-shaped particles. Here we study lollipop-shaped particles as depicted in Fig. 3.21. We model the lollipop-shaped particle as a hard spherocylinder with a hard sphere at the end of the spherocylinder. Like the hard dumbbells, the spherocylinder has a constant diameter $D = 1$ and length L. The diameter σ of the sphere is larger than the diameter of the cylinder $\sigma > D$. To compare the effect of a single sphere with the two identical spheres in the dumbbell-shaped particles we choose the same initial configuration, a close packed hexagonal AAA-crystal. In this ordering all lollipops are aligned in the same direction with all spheres in a plane in each layer. As an alternative we use the closest packed ordering for lollipops which was achieved using the floppybox Monte Carlo method [23]. Both configurations are shown in Fig. 3.22.

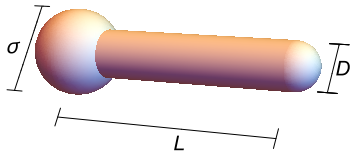

Figure 3.21: Graphical representation of a hard lollipop with cylinder length L, cylinder diameter D and sphere diameter σ.

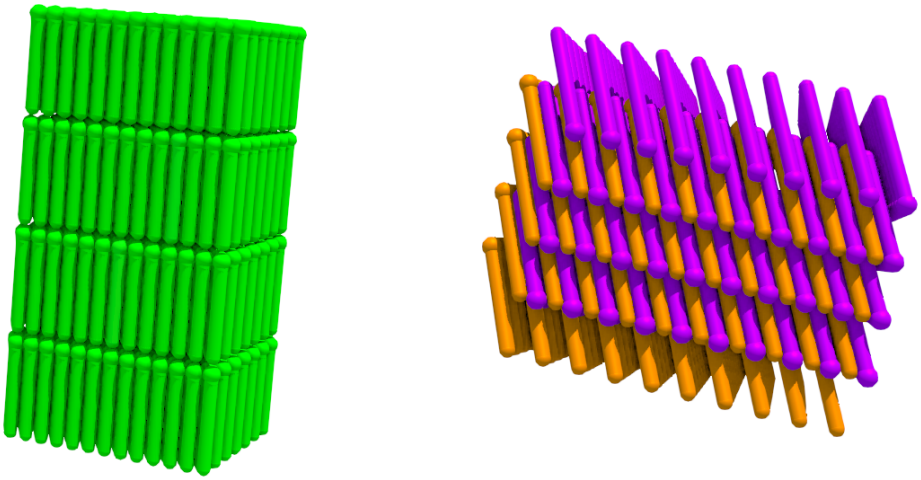

Figure 3.22: Snapshots of the initial configuration for hard lollipops with $L/D = 7$ and $\sigma/D = 1.3$ in a hexagonal AAA-crystal $\eta \approx 0.52$ (left) and a floppybox close packed configuration $\eta \approx 0.68$ provided by Nick Tasios. Particle orientations are indicated by colors. For the floppybox configuration the particles are flipped for optimal packing.

In Fig. 3.24 we present the equation of state for hard lollipops with $L/D = 7$ and $\sigma/D = 1.3$. We perform Monte Carlo simulations in the NPT-ensemble where we equilibrate the system at a fixed pressure. For each pressure we perform $5 \cdot 10^6$ Monte Carlo cycles. The different phases are identified by the nematic and smectic order parameters as shown in Sec. 3.2.1. For both the AAA-stacked initial configuration and the close packed floppybox configuration, the isotropic-nematic transition can be identified from the jumps in the nematic order parameter and packing fraction. These occur at the same packing fractions. The nematic-smectic transition is less clear due to the absence of a clear jump in packing fraction. Within the smectic range, jumps in the smectic order parameter τ, do not provide clear evidence of a smectic phase. These fluctuations could be evidence for the presence of a smectic-C phase. In a smectic-C phase the particles are tilted with respect to the layer direction whereas in a smectic-A phase they are not. Snapshots of both smectic-A and possible smectic-C ordering are shown in Fig. 3.25. Due to the tilted ordering, τ decreases. In Fig. 3.25 we can observe that the particles form smectic layers with all particles aligned in the same orientation and with particles

that are flipped due to the initial configuration. De las Heras et al. [13] observed a smectic-C phase for the top-shaped particles, which only appears for large sphere diameters, and replaces the columnar phase. For the top-shaped particles there is no smectic-A-smectic-C transition as we observe for the lollipops.

A configuration with flipped lollipops stabilizes both the nematic and smectic phase. A columnar phase is observed for both initial configurations. The smectic-columnar transition is clearly visible in the equation of state by the jump in packing fraction. For the columnar phase the nematic order parameter reaches values close to $S = 1$. The smectic order parameter drops to a low value indicating a loss in layer ordering.

An increase in the sphere diameter destabilizes the nematic, smectic and columnar phase. For hard lollipops with $L/D = 7$ and $\sigma/D > 1.4$ the smectic and columnar phase disappears when expanded from AAA-crystal initial configuration. Only short range order can be observed, as shown in Fig. 3.23. Although expanding from a close packed (floppy-box) configuration shows less defects due to the flipped particles, at high sphere diameters more defects start to appear and the different phases become more unstable. For the hard dumbbells an increase in sphere diameter stabilizes the columnar phase. Therefore the breaking of the symmetry from a dumbbell to a lollipop destabilizes the columnar phase. As we have seen for both the hard spherocylinders and dumbbells an increase in length of the cylinder stabilizes the nematic and smectic phase.

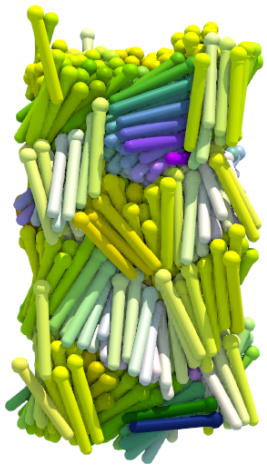

Figure 3.23: Graphical representation of hard lollipops with cylinder length $L/D = 7$ and sphere diameter $\sigma/D = 1.4$.

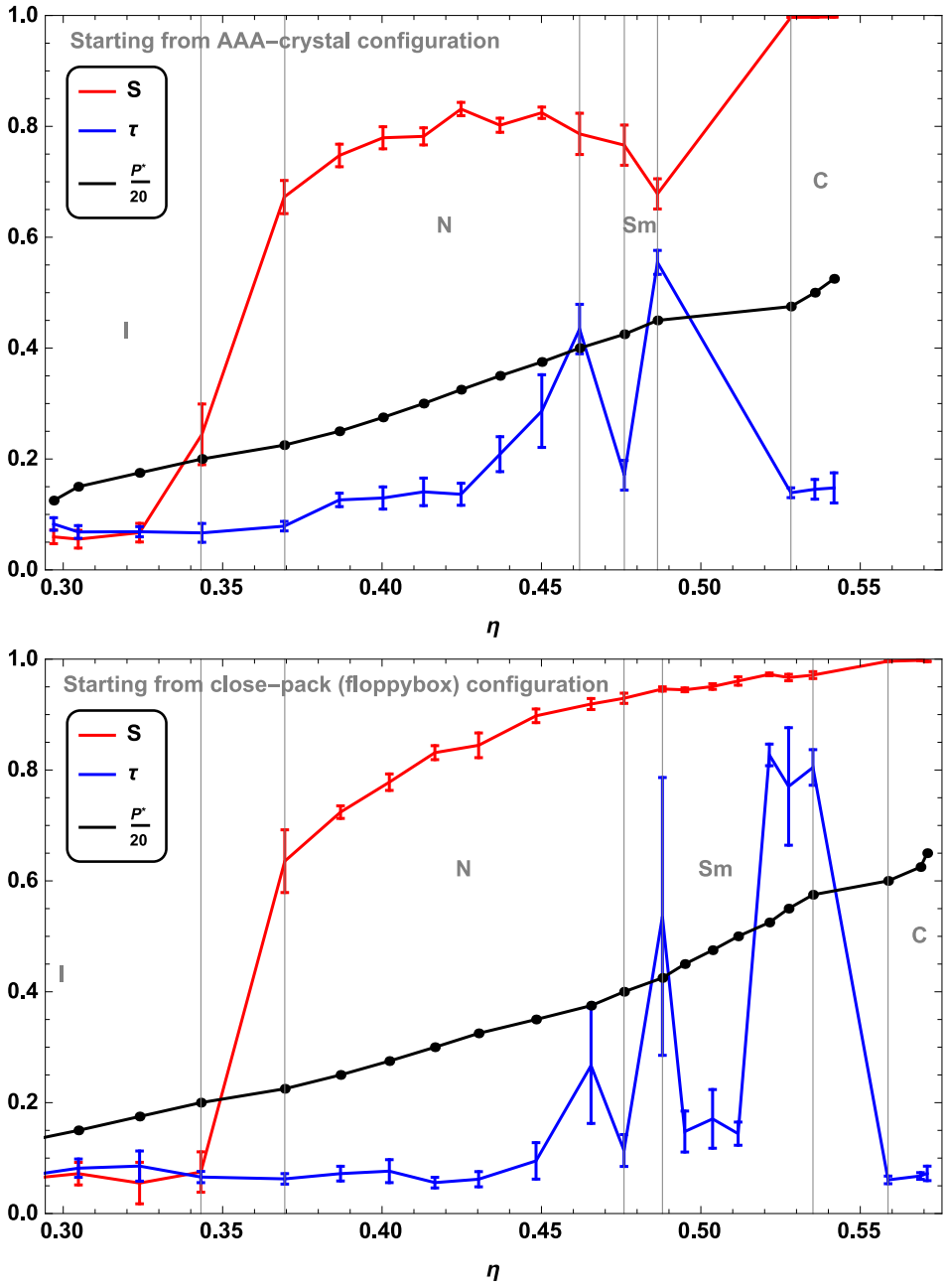

Figure 3.24: Nematic order parameter S, smectic order parameter τ and reduced pressure P^* versus the packing fraction η for hard lollipops with length $L/D = 7$ and sphere diameter $\sigma/D = 1.3$. Initial configurations are a hexagonal AAA-crystal (top) and a close packed crystal from a floppybox Monte Carlo simulation provided by Nick Tasios. Snapshots of the initial configurations are shown in Fig. 3.22. Points are joined by lines for guidance.

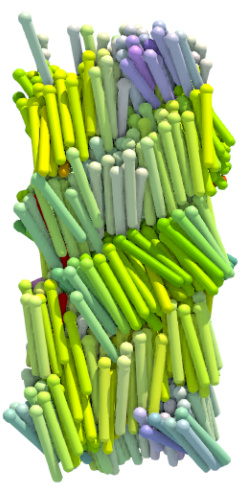

(a) $\eta \approx 0.48$

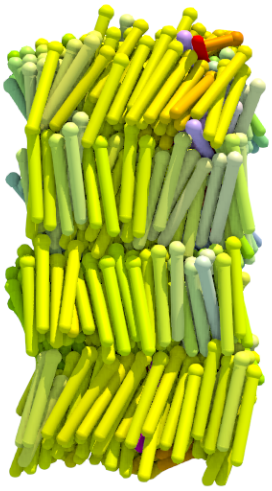

(b) $\eta \approx 0.49$

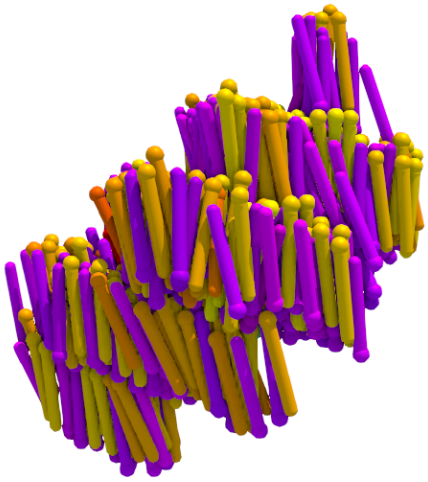

(c) $\eta \approx 0.51$

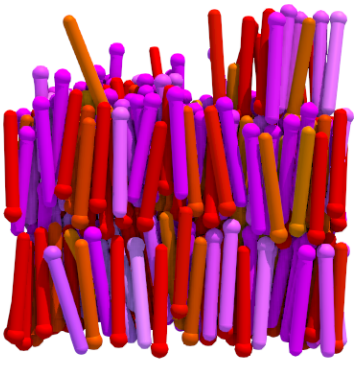

(d) $\eta \approx 0.53$

Figure 3.25: Snapshots of smectic phases for lollipops with $L/D = 7$ and $\sigma/D = 1.3$. Smectic phases are formed by expansion of an hexagonal AAA-crystal (top) and close packed crystal from a floppybox Monte Carlo simulation (bottom). Snapshots include a smectic-A phase (right) and possible smectic-C phase (left). Colors indicate the orientation of the particles.

4 Conclusion & Outlook

We have successfully simulated a solid-fluid phase transition for hard spheres using Monte Carlo simulations. The equation of state matches the theoretical approximations provided by Carnahan and Starling [15] for the fluid phase and Speedy [16] for the solid phase. We extended our model to simulate hard spherocylinders, dumbbells and lollipops. By using a linked cell list and bounding spheres we reduced the number of overlap checks thus reducing the computational times. For the hard spherocylinders we were able to reproduce the results presented by McGrother et al. [21].

For this thesis we studied the effect of the sphere diameter σ on the phase behavior of elongated dumbbells and lollipops. Our simulation results show that an increase in sphere diameter σ/D reduces the orientational entropy gain which destabilizes the nematic phase with respect to the isotropic phase. The increase of σ/D increases the packing fraction η for in-plane ordering. This destabilizes the smectic, AAA-crystal and ABC-crystal ordering but gives rise to the formation of a columnar phase. A decrease in dumbbell length reduces the nematic and smectic range. The smectic phase completely disappears for $L/D = 5$. This differs from the results for spherocylinders where the nematic phase disappears before the smectic phase.

Slowly compressing a system from the nematic phase, does not make it transition into a columnar phase. Instead short range twisted clusters are formed. These twisted clusters were predicted by de Gennes [14] and provided the possibility for a nematic cholesteric phase. The cholesteric phase was not observed in the phase diagrams from Sec. 3.3.2. We forced the system in a cholesteric phase by applying a potential to the system with cholesteric pitch q_0. After the system was equilibrated we turned the potential off and performed simulations in the NVT-ensemble for packing fractions in the nematic range. For different dumbbell lengths and sphere diameters we performed $5 \cdot 10^6$ Monte Carlo cycles. Longer dumbbells stabilize the chiral order but no evidence was found that the system was equilibrated in a cholesteric phase. Longer simulations could tell us if the system slowly equilibrates to an achiral nematic phase or to a chiral phase with some finite pitch.

For the lollipops we provided two initial configurations, an AAA-crystal and a close-packed configuration provided by a floppybox simulation. Like the dumbbells a nematic, smectic and a columnar phase were observed. The AAA-crystal is an unstable starting configuration which results in many defects in the resulting configurations. Expansion from the floppybox configuration provided two possible smectic phases. The columnar phase is first expanded to a smectic-A ordering were the nematic director is perpendicular to the smectic layering. Further expansion leads to an smectic-C phase were the particles are tilted with respect to the smectic layers. It would be interesting to see if theoretical calculations also show this smectic phase transition for hard lollipops.

References

[1] J. Seddon and R. Templer, "Polymorphism of lipid-water systems," 1995.

[2] V. Chigrinov, "Liquid crystal devices: physics and applications," *ASID'04 Tutorial notes*, 2004.

[3] S. Kokawa, M. Nishihara, and Y. Sato, "Liquid crystal display," Nov. 14 1995. US Patent 5,467,208.

[4] R. J. Witonsky and J. W. Scarantino, "Liquid crystal thermometer," July 10 2001. US Patent 6,257,759.

[5] P. Pieranski, L. Beliard, J.-P. Tournellec, X. Leoncini, C. Furtlehner, H. Dumoulin, E. Riou, B. Jouvin, J.-P. Fénerol, P. Palaric, *et al.*, "Physics of smectic membranes," *Physica A: Statistical Mechanics and its Applications*, vol. 194, no. 1, pp. 364–389, 1993.

[6] R. Brown, "Xxvii. a brief account of microscopical observations made in the months of june, july and august 1827, on the particles contained in the pollen of plants; and on the general existence of active molecules in organic and inorganic bodies," *Philosophical Magazine Series 2*, vol. 4, no. 21, pp. 161–173, 1828.

[7] G. M. Whitesides and B. Grzybowski, "Self-assembly at all scales," *Science*, vol. 295, no. 5564, pp. 2418–2421, 2002.

[8] N. Metropolis, A. W. Rosenbluth, M. N. Rosenbluth, A. H. Teller, and E. Teller, "Equation of state calculations by fast computing machines," *The journal of chemical physics*, vol. 21, no. 6, pp. 1087–1092, 1953.

[9] D. Frenkel, "Order through disorder: entropy-driven phase transitions," in *Complex Fluids*, pp. 137–148, Springer, 1993.

[10] P. Bolhuis and D. Frenkel, "Tracing the phase boundaries of hard spherocylinders," *Journal of chemical physics*, vol. 106, no. 2, pp. 666–687, 1997.

[11] C.-J. Huang, P.-H. Chiu, Y.-H. Wang, and C.-F. Yang, "Synthesis of the gold nanodumbbells by electrochemical method," *Journal of colloid and interface science*, vol. 303, no. 2, pp. 430–436, 2006.

[12] B. Peng, G. Soligno, M. Kamp, B. De Nijs, J. De Graaf, M. Dijkstra, R. Van Roij, A. Van Blaaderen, and A. Imhof, "Site-specific growth of polymers on silica rods," *Soft matter*, vol. 10, no. 48, pp. 9644–9650, 2014.

[13] D. de las Heras, S. Varga, and F. J. Vesely, "Mesophase formation in a system of top-shaped hard molecules: Density functional theory and monte carlo simulation," *The Journal of chemical physics*, vol. 134, no. 21, p. 214902, 2011.

[14] J. Prost, *The physics of liquid crystals*. No. 83, Oxford university press, 1995.

[15] N. F. Carnahan and K. E. Starling, "Equation of state for nonattracting rigid spheres," *The Journal of Chemical Physics*, vol. 51, no. 2, pp. 635–636, 1969.

[16] R. Speedy, "Pressure and entropy of hard-sphere crystals," *Journal of Physics: Condensed Matter*, vol. 10, no. 20, p. 4387, 1998.

[17] M. N. Bannerman, L. Lue, and L. V. Woodcock, "Thermodynamic pressures for hard spheres and closed-virial equation-of-state," *The Journal of chemical physics*, vol. 132, no. 8, p. 084507, 2010.

[18] L. Onsager, "The effects of shape on the interaction of colloidal particles," *Annals of the New York Academy of Sciences*, vol. 51, no. 4, pp. 627–659, 1949.

[19] D. Frenkel, H. Lekkerkerker, and A. Stroobants, "Thermodynamic stability of a smectic phase in a system of hard rods," 1988.

[20] C. Vega and S. Lago, "A fast algorithm to evaluate the shortest distance between rods," *Computers & chemistry*, vol. 18, no. 1, pp. 55–59, 1994.

[21] S. C. McGrother, D. C. Williamson, and G. Jackson, "A re-examination of the phase diagram of hard spherocylinders," *The Journal of chemical physics*, vol. 104, no. 17, pp. 6755–6771, 1996.

[22] J. Veerman and D. Frenkel, "Relative stability of columnar and crystalline phases in a system of parallel hard spherocylinders," *Physical Review A*, vol. 43, no. 8, p. 4334, 1991.

[23] L. Filion, M. Marechal, B. van Oorschot, D. Pelt, F. Smallenburg, and M. Dijkstra, "Efficient method for predicting crystal structures at finite temperature: variable box shape simulations," *Physical review letters*, vol. 103, no. 18, p. 188302, 2009.